Structural and Biochemical Characterization of Rm3, a SubClass B3 Metallo-β-Lactamase Identified from a Functional Metagenomic Study

Ramya Salimraj[1], Lihong Zhang[2,3*], Philip Hinchliffe[1], Elizabeth M. H.Wellington[2], Jürgen Brem[4], Christopher J. Schofield[4], William H. Gaze[2,3*] and James Spencer[1#]

[1]School of Cellular and Molecular Medicine, University of Bristol Medical Sciences Building, University Walk, Bristol BS8 1TD, United Kingdom.

[2]School of Life Sciences, University of Warwick, Coventry CV4 7AL, United Kingdom

[3]European Centre for Environment and Human Health, University of Exeter Medical School, Knowledge Spa, Royal Cornwall Hospital, Truro, Cornwall TR1 3HD, UK

[4]Department of Chemistry, University of Oxford, 12 Mansfield Road, Oxford, OX1 3TA, United Kingdom

[*]present address

[#]Correspondence and reprints.

Mailing address for James Spencer: School of Cellular and Molecular Medicine, University of Bristol, Biomedical Sciences Building, University Walk, Bristol BS8 1TD, United Kingdom.

Phone: (44) (0) 117 331 2084.

Fax: (44) (0) 117 331 2091.

E-mail: Jim.Spencer@bristol.ac.uk

Running Title: Characterization of Rm3 metallo-β-lactamase

Abstract

β-Lactamase production increasingly threatens the effectiveness of β-lactams, which remain a mainstay of antimicrobial chemotherapy. New activities emerge both through mutation of previously known β-lactamases and mobilization from environmental reservoirs. The spread of metallo-β-lactamases (MBLs) represents a particular challenge through their typically broad spectrum activities, encompassing carbapenems in addition to other β-lactam classes. Increasingly, genomic and metagenomic studies reveal distribution of putative MBLs in the environment, but in most cases their activity against clinically relevant β-lactams, and hence the extent to which they can be considered a resistance reservoir, remains uncharacterized. Here we characterize the product of one such gene, bla_{Rm3}, identified through functional metagenomic sampling of an environment with high biocide exposure. bla_{Rm3} encodes a subclass B3 MBL that, when expressed in recombinant *E. coli*, is exported to the bacterial periplasm and hydrolyzes clinically used penicillins, cephalosporins, and carbapenems with an efficiency limited by high K_M values. An Rm3 crystal structure reveals the MBL superfamily αβ/βα fold, which more closely resembles mobilized B3 MBLs (AIM-1, SMB-1) than other chromosomal enzymes (L1 or FEZ-1). A binuclear zinc site sits in a deep channel that is in part defined by a relatively extended N-terminus. Structural comparisons suggest that the steric constraints imposed by the N-terminus may limit β-lactam affinity. Sequence comparisons identify Rm3-like MBLs in numerous other environmental samples and species. Our data suggest that Rm3 like enzymes represent a distinct group of B3 MBLs with a wide distribution and can be considered as an environmental reservoir of β-lactam resistance.

Introduction

The continued efficacy of β-lactam antibiotics is threatened by the dissemination of β-lactamases, hydrolytic enzymes that inactivate these important drugs by cleavage of the scissile β-lactam amide bond (1). In the 70 years since β-lactams were first introduced to the clinic, repeated mobilizations of β-lactamase genes from a variety of bacterial sources have led to their rapid propagation in opportunistic Gram-negative pathogens such as the Enterobacteriaceae and non-fermenting species including *Pseudomonas aeruginosa* and *Acinetobacter baumannii* (2). Notably, some of the most successful β-lactamases, in particular the CTX-M extended-spectrum β-lactamase (ESBL) associated with resistance to third-generation cephalosporins such as cefotaxime, and which is now distributed worldwide (3), find their origins in environmental organisms, illustrating how transfer of antibiotic resistance genes from environmental to pathogenic species can have profound clinical consequences (4). In the case of CTX-M enzymes it is now accepted that these originated in *Kluyvera* spp. (5, 6), a Gram-negative rod bacterium that is found in both the human intestinal microbiome and the wider natural environment (7).

β-Lactamases are divided, primarily on the basis of amino acid sequence, into four main classes (8). Of these, three (classes A, C and D) are active site nucleophilic serine enzymes (SBLs) and the remaining class, B, zinc metalloenzymes that are structurally and mechanistically unrelated to the SBLs. The metallo-β-lactamases (MBLs) are themselves divided into a further three groups (B1, B2 and B3) on the basis of sequence differences that are manifest as variations in the number (1 or 2) of zinc ions required for full activity, and in structural differences that include variations in co-ordination of the active site zinc ions (9, 10). MBLs are a growing clinical concern as they effectively hydrolyze all β-lactam classes excepting the monobactams and

escape the action of SBL inhibitors (11) that are at (clavulanate, tazobactam) or close to (avibactam, relebactam) the clinic. B1 MBLs such as the NDM (12) and VIM (13) enzymes are now encountered with increasing frequency on mobile genetic elements in organisms such as *Escherichia coli*, *Klebsiella pneumoniae*, *P. aeruginosa* and *A. baumannii*.

While B3 family members such as AIM-1 (14) and SMB-1 (15) have been identified on mobile genetic elements, the majority of these enzymes are chromosomal. However, in addition to their presence in opportunist pathogens such as *Stenotrophomonas maltophilia* (16) and *Elizabethkingia meningosepticum* (17), the B3 MBLs also have a very wide distribution in environmental organisms and sequences. Compared to the B1 enzymes, the B3 MBLs are less well studied, display a greater degree of structural and sequence diversity and are more closely related to other branches of the wider metallo-hydrolase superfamily to which the MBLs belong (18). Investigations of B3 MBLs from environmental sources will thus expand our understanding of activity and structure within this group of enzymes and provide insights into the nature and extent to which MBLs in the environment provide a reservoir of resistance determinants to the most clinically important β-lactam antibiotics. Furthermore, identifying how the distribution of such sequences changes in response to human activity (i.e. exposure to antimicrobials within the environment) can also provide evidence of the effect of human activity upon the environmental resistance reservoir (19).

Technological advances have transformed our ability to sample and identify antibiotic resistance genes in the natural environment. In particular, combining sequence-based (metagenomics) with functional (construction and analysis of large libraries) methodologies can both establish the prevalence and distribution of putative resistance genes and identify those that confer a resistance phenotype, i.e that are able to alter antibiotic susceptibility in a model organism (e.g.

E. coli) (20-22). This study provides a biochemical and structural characterization of a B3 MBL, Rm3, that was identified by application of this functional metagenomics approach to study the distribution of resistance to third-generation cephalosporins in environmental sources selected on the basis of differing degrees of human impact. (Full details of the identification of Rm3 will be presented elsewhere). The bla_{Rm3} gene (GenBank accession KF485393.2) was isolated from a metagenomic library derived from soil from a reed bed used to bioremediate effluent from a textile mill with high usage of quaternary ammonium compounds (QACs). Screening of this library identified bla_{Rm3} as one of a number of novel β-lactamase genes able to decrease susceptibility of recombinant *E. coli* to third generation cephalosporins.

The Rm3 amino acid sequence (Figure 1) most closely resembles other putative B3 MBLs from environmental bacteria, in particular sequences from the soil bacteria *Janthinobacterium* (e.g. GenBank KKO63914.1; 89 % sequence identity (23)) and *Solimonas* (e.g. NCBI accession WP_020650668.1; 56 % identity) *spp*. Rm3 also resembles (54 % sequence identity) a novel B3 MBL, LRA-8, identified from a metagenomics study of the Tanana river in Central Alaska (20) (Figure 1), and a related sequence (GenBank AIA12579.1; 56 % identity) identified from a grassland soil sample from Minnesota, U.S.A., as part of a functional metagenomics study of environmental antibiotic resistance genes (24). Of biochemically characterized B3 MBLs, Rm3 shares the highest sequence identity with THIN-B (25) (49%) and is between 43% (SMB-1) (15) and 27% (BJP-1) (26) identical to enzymes of known structure. On this basis, (Figures 1,2), Rm3 can be considered as being representative of a group of uncharacterized novel B3 MBLs that appear to be widely distributed within the environmental microbiome. Here we present the biochemical and structural characterization of recombinant Rm3.

Materials and Methods

Identification of *bla*$_{Rm3}$

Full details of the identification of Rm3 will be presented elsewhere. Briefly, core samples were obtained from reed beds used for remediation of effluent from a textile mill in Yorkshire, U.K., (27) and total DNA was purified as previously described (21). A metagenomic library was generated by cloning purified DNA fragments into plasmid pCF430 (28) and transforming into *E. coli* strain EC100 (Epicentre, Madison WI, U.S.A.) by electroporation. Recombinants were passaged over 10-20 generations and clones resistant to third generation cephalosporins selected by plating on ceftazidime (1 µg / ml). Putative resistance genes were identified by sequencing positive clones, and their contribution to the resistance phenotype confirmed by inactivation using transposon mutagenesis (EZ-Tn5 kit, Epicentre) allowing for selection by loss of phenotype (21).

Minimal Inhibitory Concentration (MIC) Determination for Metagenomic Clones

Minimal inhibitory concentration (MIC) values for metagenomic clones were determined by agar dilution on Iso-sensi Test Agar (Oxoid) with an inoculum of 10^5 colony forming units (cfu) per spot (29).

Recombinant Rm3 Expression and Purification

The complete Rm3 open reading frame (including the putative periplasmic export sequence) was amplified from metagenomic clone RM3 by PCR with primers RM3F

(AAGGCATATGATGTCCCTCACACCACCACGCGCG) and RM3R2(AATGGGATCCTTAC TGCTGTTTTTCCTGGT) with proof-reading Pfu DNA polymerase. The product was ligated into the T7 expression vector pET26b (30) using the Nde1 and BamH1 restriction sites and the integrity of the resulting plasmid pLHZRM3 confirmed by DNA sequencing. *E. coli* ArcticExpress (DE3) competent cells (Agilent, Stockport, U.K.) transformed with pLHZRM3 were grown (Power Broth (Athena Enzyme Systems, Baltimore, MD, U.S.A.); 30° C; 160 rpm shaking) to OD_{600nm} ≈ 0.6 and expression induced overnight (1 mM isopropyl-β-D-thiogalactopyranoside (Melford Laboratories, Ipswich, U.K.); 13° C). Cells were harvested by centrifugation (7 205 g; 30 mins; 4° C) and lysed in a Constant Systems (Daventry, U.K.) cell disruptor (25 000 psi). Debris was removed by centrifugation (38 724 g, 1 h) and the supernatant exchanged into buffer A (50 mM potassium phosphate pH 7.0, 1 M ammonium sulfate) by extensive dialysis using a 3 000 Da cut-off membrane (Medicell International, London, U.K.).

Protein for crystallography was purified by the following method. 20 ml of the dialysate was loaded on a 1 ml Phenyl FF HS column (GE Healthcare Life Sciences, Little Chalfont, U.K.) and the column washed consecutively with buffer B (buffer A plus 10 mM $MgCl_2$, 5 mM ATP, 50 mM KCl) and buffer A prior to elution on a gradient of 0 – 50 % buffer C (50 mM potassium phosphate pH 7.0). Rm3-containing fractions were identified by SDS-PAGE (31) and concentrated to a volume of ~2 ml by centrifugal ultrafiltration using an Amicon concentrator with a 3 000 Da molecular weight cut off (Millipore, Watford, U.K.). Protein was loaded onto a 300 ml Superdex S75 size exclusion column (GE Healthcare) and eluted with a flow rate of 1 ml / min in buffer D (20 mM Tris pH 7.5, 200 mM NaCl). Rm3-containing fractions were pooled and concentrated as above.

For enzyme kinetic experiments Rm3 was purified by a modified version of the above protocol where recombinant protein was produced in *E. coli* SoluBL21 cells (AMS Biotechnology, Abingdon, U.K.) that were grown overnight in Autoinduction Terrific Broth (Formedium, Hunstanton, U.K.) at 25° C. The hydrophobic interaction chromatography step utilized a 40 ml Phenyl FF HS column, omitted the ATP wash and eluted bound protein on a 0 – 100 % buffer C gradient; and size exclusion chromatography utilized a 120 ml HiLoad 16/60 Superdex 75 pg column (GE Healthcare).

Verification of Recombinant Rm3 by Mass Spectrometry

ESI mass analyses were acquired (as described (32)) in the positive ion mode using a Waters (Elstree, U.K.) LCT Premier instrument equipped with a TOF analyzer. An LCT Premier mass spectrometer (Waters) was coupled to an Agilent 1100 Series HPLC using a Chromolith® FastGradient RP-18 endcapped column equipped with a 50-2 HPLC column, made of monolithic silica (C18, 2 x 50 mm, macropores with 1.6 µm diameter, Merck (Beeston, U.K.)). The instrument was connected to a CTC-autosampler inlet system. A multi-step gradient over 10 min was run (solvent A 94.9% H_2O/5% CH_3CN/0.1% formic acid, solvent B 99.9% CH_3CN/0.1% formic acid; 0-1 min 5% B for equilibration, followed by a linear gradient to 100% B over 4 min, then 100% B for an additional 3 min, followed by a linear gradient over 2 min back to 5% B to re-equilibrate the column) to separate the protein samples at flow rates of 0.4 ml / min for the first 5 min and then 1.0 ml / min for the remaining time. The electrospray ionization source used a capillary voltage of 3.2 kV and cone voltage of 25 V. Nitrogen was used as the nebulizer and desolvation gas at a flow rate of 600 l/h. Protein typically eluted as a peak

between 3 and 5 min under these conditions. Calculated masses were obtained using the ExPasy ProtParam tool (http://web.expasy.org/protparam/ (33)).

Steady-State Kinetics of β-Lactam Hydrolysis by Recombinant Rm3

Hydrolysis of selected β-lactams by recombinant Rm3 was investigated under steady-state conditions. The buffer was 50 mM HEPES, pH 7.0, supplemented with 100 μM $ZnCl_2$ and 100 μg/ml BSA and the protein concentration was 10 nM. Measurements used either a Polarstar Omega plate reader (BMG LabTech, Aylesbury, U.K.) or, for complete hydrolysis curves, a Lamda 35 spectrophotometer (Perkin-Elmer, Seer Green, U.K.). Extinction coefficients and wavelengths used (34) were: -775 M^{-1} cm^{-1} at 235 nm (penicillin G); -820 M^{-1} cm^{-1} at 235 nm (ampicillin); -7700 M^{-1} cm^{-1} at 260 nm (cefoxitin); -9000 M^{-1} cm^{-1} at 260 nm (ceftazidime); -7500 M^{-1} cm^{-1}-at 260 nm (cefotaxime); - 6500 M^{-1} cm^{-1} at 300 nm (meropenem); - 9000 M^{-1} cm^{-1} at 300 nm (imipenem); and -700 M^{-1} cm^{-1} at 320 nm (aztreonam).

Data were analyzed by fitting to the Michaelis-Menten equation:

$$V = k_{cat}*[E]*[S] / (K_M + [S])$$

Where V is the measured initial velocity at substrate concentration [S] and [E] is the concentration of enzyme. Where high apparent K_M values precluded data collection under the conditions required to achieve saturation of hydrolysis rate, the value of k_{cat}/K_M was measured by fitting progress curves (absorbance versus time) for a complete hydrolysis reaction to the exponential:

$$A_t = A_\infty + (A_0 - A_\infty)*e^{-kt}$$

where A_t is the absorbance at time t and A_0 the initial and A_∞ the final absorbance. The observed first-order rate constant is then k = (k_{cat}/K_M)*[E] (35). Curve fitting was undertaken using Prism (GraphPad, La Jolla, CA, U.S.A.).

Rm3 Crystallization and Structure Determination

Purified Rm3 protein in buffer D was concentrated to ~13 mg / ml by ultracentrifugation as above and supplemented with 100 µM $ZnCl_2$ and 5 mM Tris(2-carboxyethyl)phosphine (TCEP) hydrochloride (Fisher Scientific). Initial crystallization hits were obtained from commercial sparse matrix screening kits (Molecular Dimensions (Newmarket, U.K.) Proplex (36)) using a Phoenix crystallization robot (Art Robbins Instruments, Sunnyvale, CA, U.S.A.) to set 100 nl plus 100 nl sitting drops in 96-well MRC plates (Molecular Dimensions) using a reservoir volume of 100 µl. Conditions were optimized using 1 µl plus 1 µl hanging drops in 24-well XRL plates (Molecular Dimensions) with 500 µL reservoir volume. Diffraction data were collected from a single crystal grown in a hanging drop from 14% w/v PEG 8000, 0.1 M Tris pH 8, 0.15 M LiCl. All crystallization experiments were carried out at 18 °C.

The Rm3 crystal was cryoprotected for ~30 seconds by exposure to reservoir solution supplemented with 25% ethylene glycol, mounted in a SPINE standard pin (Molecular Dimensions) and flash frozen in liquid nitrogen. Diffraction data were collected on beamline I04 of the Diamond Light Source (DLS), U.K., using a Pilatus 6M-F detector. 934 images of 0.15° oscillation (exposure 0.15 s per image; 20% beam intensity) were collected at a wavelength of 0.9795 Å. Diffraction data were integrated using XDS (37), the space group was identified using Pointless (38) and data were scaled and merged using Aimless (38) as implemented in the Xia2

pipeline (39). The structure was solved by molecular replacement using Phaser (40) with Chainsaw (41) used to create a search model based upon *S. maltophilia* L1 (chain A of PDB 2QDT (42)) by pruning side chains of non-identical amino acids to their Cγ atoms. Models were built in Coot (43) and refinement carried out using Refmac 5 (44). Final refinement and model validation (MolProbity (45)) took place in Phenix (46).

Coordinates and structure factors have been deposited in the Protein Data Bank (www.rcsb.org/pdb) with accession no. 5IQK.

Results and Discussion

Identification of Rm3 as a Subclass B3 Metallo-β-Lactamase

bla$_{Rm3}$ was identified by selecting ceftazidime resistant clones from a metagenomic library constructed from DNA purified from samples originating from a reed bed used to bioremediate effluent from a textile mill with high usage of quaternary ammonium compounds (QACs). QACs are disinfective agents with wide industrial application, and have been implicated in the selection of co- and cross-resistance to a variety of antibiotic classes, including β-lactams (47, 48). *bla*$_{Rm3}$ was situated on an 8 kb DNA fragment (metagenomic clone RM3; GenBank accession KF485393.2) that exerted variable effects upon susceptibility to β-lactam antibiotics but that resulted in a 16-fold elevation of the MIC of *E. coli* EC100 to CAZ (ceftazidime) compared to vector-only control (Table 1). This effect was abolished by insertional inactivation of *bla*$_{Rm3}$ by transposition (data not shown). The amino acid sequence of the *bla*$_{Rm3}$ encoded protein, Rm3, showed properties (presence of a His116-Xaa-His118-Xaa-Asp120-His121 sequence motif and similarity to previously characterized enzymes) characteristic of a subclass B3 MBL (Figure 1).

Expression and Kinetic Characterization of Recombinant Rm3

The *bla*$_{Rm3}$ gene encodes a 302 residue polypeptide that includes an N-terminal leader peptide of 23 residues that was identified by SignalP (49) as a periplasmic export sequence. The complete Rm3 open reading frame, including the putative export sequence, was expressed in either *E. coli* ArcticExpress or SoluBL21 and was purified to apparent homogeneity by hydrophobic interaction and size exclusion chromatography. Quadrupole time-of-flight (QTOF) mass spectrometry under denaturing conditions gave a mass of 29 805 Da for the purified protein,

consistent with a predicted mass of 29 808.5 Da for the Rm3 fragment resulting from removal of the predicted precursor polypeptide after residue 23. Thus these data confirm that the leader peptide is removed from recombinant Rm3 by post-translational processing in *E. coli*, and strongly indicate that, as is the case for other β-lactamases of Gram-negative bacteria, the protein is exported to the bacterial periplasm.

Steady-state kinetic experiments indicate that Rm3 is able to hydrolyze a range of penicillin, cephalosporin, and carbapenem antibiotics with varying degrees of efficiency (Table 2). Notably, it was possible to obtain accurate K_M estimates for only two substrates, meropenem and ampicillin, of the eight that were evaluated. For the other substrates tested it proved difficult to saturate the Michaelis-Menten (i.e. rate versus substrate concentration) plots, indicating high K_M values and likely low affinity. For these substrates, values for catalytic efficiency (k_{cat}/K_M) only are reported. Overall catalytic efficiencies approaching 10^5 M^{-1} s^{-1} are achieved for substrates from all classes excepting the monobactam aztreonam, against which Rm3, as is the case for other MBLs, shows no hydrolytic activity. These data show Rm3, in common with most other B3 MBLs, to be an enzyme with a broad spectrum of activity. The relatively low catalytic efficiencies that are achieved by Rm3, compared to other characterized B3 MBLs where values for k_{cat}/K_M in excess of 10^7 M^{-1} s^{-1} have been reported for some favorable enzyme:substrate combinations (e.g. AIM-1-catalyzed imipenem hydrolysis (14)), arise primarily from the relatively high K_M values. For all substrates tested K_M values were 10^{-4} M or above, contrasting with most other B3 MBLs where for more favored substrates K_M values of 10^{-5} M or better are obtained. Some other enzymes from environmental sources, such as *J. lividum* BJP-1 (26), *Erwinia caratovora* CAR-1 (50) and *Caulobacter crescentus* CAU-1 (51), are also notable for comparably high K_M values across the range of β-lactams. However, Rm3 is distinguished from

Antimicrobial Agents and Chemotherapy

many of these by an apparent lack of discrimination against oxyiminocephalosporins (e.g. ceftazidime) or 7-α-methoxy cephalosporins (e.g. cefoxitin) that are poor substrates for the B3 enzymes CAR-1 and CAU-1, respectively. k_{cat}/K_M values for hydrolysis of these substrates by Rm3 are in line with those for other β-lactams tested.

Crystal Structure of Rm3

Rm3 crystallized in space group $P2_1$ with two molecules in the asymmetric unit. A single 1.75 Å resolution dataset was collected at the Diamond Light Source synchrotron radiation facility and phases and an initial electron density map calculated by molecular replacement. Data collection and refinement statistics are given in Table 3. The final structure contains 268 (chain A) and 269 (chain B) residues, with electron density not observed for the 10 (chain A) or 9 (chain B) N-terminal amino acids, or for the C-terminal glutamine residue of either polypeptide chain. We note that the N-terminus of processed Rm3 is formed by a proline-rich sequence (QTPAPATPP) that is likely to be unstructured in solution. 96.6 % of total residues are in the most favored regions of the Ramachandran plot, with no residues classed as outliers. The overall structure (Figure 3) is that of the MBL superfamily, comprising an αβ / βα fold in which the N- and C-terminal halves of the protein form central seven- and five-stranded β-sheets, respectively, that are flanked by α-helices. The interface of these two sheets provides the location for the active site. The active site environment is defined by three loop regions that connect elements of secondary structure: residues 150 – 164 (loop 1) connecting helix α4 and strand β7; residues 192 – 201 that connect strands β9 and β10 and residues 222 – 239 (loop 2) connecting strand β11 and helix α5. (The BBL numbering scheme (52) is used throughout this manuscript).

Antimicrobial Agents and Chemotherapy

The presence of disulfide bonds also serves to define the overall architecture of the Rm3 structure. The processed Rm3 polypeptide contains a total of 6 Cys residues, of which two (residues 256 and 290) form a disulfide bond between helices α5 and α7 that is common to all B3 MBLs of known structure excepting BJP-1 (53). In chain A of the current structure a second disulfide between Cys208 and Cys213 constrains the short loop between strands β10 and β11. However, in chain B this disulfide bond is not present, Cys208 and Cys213 are reduced and a zinc ion is positioned between them. This zinc ion is also coordinated by His246 and Glu249 of an adjacent chain and thus occupies a site that is formed at the interface of two Rm3 monomers in adjacent asymmetric units in the crystal. The final pair of Cys residues (positions 32 and 35) also contribute to a further zinc site at the interface between the two Rm3 molecules present in the crystallographic asymmetric unit, in which zinc co-ordination is completed by His158 of the opposing chain, and by a crystallographic water molecule. However, as Rm3 eluted from the size exclusion chromatography column at a volume consistent with a molecular weight of approximately 30 000 Da (data not shown), indicating that the protein is likely to exist as a monomer in solution, we consider both of these interface sites to be crystallization artefacts that are unlikely to exert a physiological function.

Inspection of difference electron density maps from the early stages of refinement unambiguously identified the presence of two metal ions in the Rm3 active site. These were refined as zinc ions, based upon the presence of excess zinc in the crystallization experiment and the absence of other metal ions in the crystal as adjudged by the lack of additional peaks in an X-ray fluorescence excitation spectrum collected at the synchrotron beamline (data not shown). Both sites were refined to 100 % occupancy with B-factors similar to those of the adjacent protein atoms (Table 3). Consistent with assignment of Rm3 as a member of the B3 MBL

subfamily, the two zinc ions respectively occupy the two binding sites that are defined by conserved residues of the MBL superfamily; i.e. a tri-histidine (Zn1) site formed by His116, His118 and His196 and an Asp – His – His (Zn2) site formed by Asp120, His121 and His263 (Figure 4). In both subunits the two zinc ions lie approximately 3.5 Å apart (distances 3.46 Å and 3.51 Å in chains A and B, respectively) and are connected by a "bridging" water molecule (Wat1, likely to exist as an hydroxide ion (54)) that is positioned asymmetrically with respect to the two metal ions and lies closer to Zn1 (1.81 - 1.90 Å) than to Zn2 (2.04 - 2.11 Å). Metal co-ordination is completed by a second water molecule (Wat2) that lies closer to Zn2 but also co-ordinates Zn1 (Wat2 – Zn1 distances 2.57 and 2.68 Å in chains A and B, respectively), and can thus also be considered to bridge the two metal ions. In consequence both Rm3 metal ions are five co-ordinated.

Five co-ordinate metal ion systems can be described using the structural parameter τ (τ = (β - α)/60) to discriminate between trigonal (τ = 1) and square (τ = 0) pyramidal geometries (55). For the Rm3 Zn1 site the two angles α and β that represent distortion from square to trigonal bipyramidal co-ordination can be defined as His116 – Zn1 – His196 (103.5º) and Wat2 – Zn1 – His118 (167.4º), respectively (56), yielding a value for τ of 1.07 and indicating that co-ordination is best described as trigonal bipyramidal. For the Zn2 site α and β are defined as Wat1 – Zn2 – His263 (127.4º) and Wat2 – Zn2 – Asp120 (155.9º), respectively (57), giving τ = 0.475 and co-ordination geometry as intermediate between trigonal bi- and square pyramidal. In chain B Wat2 is less well defined by the experimental electron density but occupies a similar position, with values for τ of 0.97 for the Zn1, and 0.41 for the Zn2, sites. Thus zinc co-ordination is similar in both Rm3 molecules.

337

338 **Comparison with Other B3 MBL Structures**

339 PDBeFold (58) was used to generate superpositions of chain B of Rm3 with five other B3 MBLs
340 of known crystal structure: L1 (pdb 1SML (59), RMSD 1.47 Å over 240 Cα atoms), FEZ-1 (pdb
341 1K07 (60). RMSD 1.65 Å over 254 Cα atoms), BJP-1 (pdb 3LVZ (53), RMSD 1.73 Å over 251
342 Cα atoms), AIM-1 (pdb 4AWY (61), RMSD 1.04 Å over 247 Cα atoms) and SMB-1 (pdb 3VPE
343 (57), RMSD 0.87 Å over 245 Cα atoms). Thus, the Rm3 structure most closely resembles those
344 of AIM-1 and SMB-1, consistent with the closer sequence relationship to these enzymes than to
345 other structurally characterized B3 MBLs. Superposition of the B3 MBL structures (Figure 5)
346 identifies three regions where there is variation between the various structures - the extreme N-
347 terminus, the loop connecting helix α4 and strand β7 (sometimes termed loop1) and that
348 connecting strand β11 and helix α5 (loop2 (57)). Together these three regions substantially
349 define the active site groove in B3 MBLs. Notably, the N-terminal region of Rm3 is poorly
350 defined in the crystal structure, with no electron density evident for the proline-rich sequence
351 (QTPAPATPP) that forms the N-terminus of the processed polypeptide after cleavage of the
352 signal peptide. However, unlike the AIM-1 and SMB-1 structures, where a turn preceding the
353 conserved Trp41 forces relatively short N-termini away from the active site, in Rm3 Trp41 is
354 part of an α-helix (α1, Figure 3) that defines one wall of a deeper active site groove (Figure 5).
355 Thus, in this regard Rm3 more closely resembles BJP-1, where an extended helical N-terminus
356 creates an active site that is much narrower than those of other B3 MBLs of known structure.

357 Loop1 (residues 150 – 164) of B3 MBLs also contributes substantially to the active site
358 architecture. Hydrophobic residues (Phe156 and Ile162) in loop1 of L1 were proposed to

participate in binding of substrate (59), but subsequent directed mutagenesis investigations of L1 (62) and FEZ-1 (63) did not identify these individual positions as essential to activity. However, rapid kinetic experiments (64) demonstrate that this loop can adjust its position during turnover of β-lactams by the L1 enzyme, indicating that the structure as a whole may have some mechanistic role. In addition, both AIM-1 and SMB-1 feature a Gln at position 157, where models of bound cephalosporin substrates suggest that it may interact with the carboxylate group at C7/C8 formed on hydrolysis of the β-lactam amide (57, 61). In Rm3 Gln157 is present, as part of a DPQ motif that is also found in SMB-1, AIM-1 and THIN-B, and the organization of loop1 closely resembles that found in AIM-1 and SMB-1 (Figure 5). By way of contrast, loop1 in the L1, FEZ-1 and BJP-1 structures adopts a more "open" conformation than is the case here.

Loop2 (residues 224 - 230) is the third region of variability between B3 MBL structures. In common with AIM-1 and SMB-1, loop2 of Rm3 is longer by two residues than its equivalent in other B3 enzymes, with the apex of this loop extending away from the active site. In L1 and FEZ-1, residues such as Asn225 (FEZ-1) and Tyr228 (both enzymes) on loop2 are proposed to contribute to β-lactam hydrolysis through interaction with the C7/C8 carboxylate group of hydrolyzed species (see above) (59, 60, 62). Consistent with the presence of Gln157 on loop1 (see above) which could act as a functional replacement for these residues, the equivalent positions of Rm3 loop2 are occupied by amino acids (Val and Pro) that are unable to replicate these proposed interactions, and the conformation of loop2 is also incompatible with a contribution to β-lactam binding and/or hydrolysis. Loop2 of BJP-1 also differs from the equivalent regions of L1 and FEZ-1, but in this case it is positioned in a more "closed" conformation nearer to the zinc center. Taken together, these comparisons indicate that, in both the overall fold, and the specific architecture of variable regions (loops 1 and 2) adjacent to the

active site, the Rm3 structure more closely resembles that of the mobile B3 enzymes AIM-1 and SMB-1 than it does the chromosomal B3 MBLs L1, FEZ-1 and BJP-1.

In contrast to these clear differences in overall structure between different B3 MBLs, comparison of the respective active sites indicates that the principal features of the Rm3 metal center are common between all structurally characterized B3 MBLs. Specifically, all B3 MBLs of known structure feature a binuclear zinc center with a five co-ordinate ion in the Zn2 site and geometry intermediate between trigonal bi- and square pyramidal, and (for structures that do not contain bound ligands) the zinc – zinc distance (3.46 Å and 3.51 Å in Rm3 chains A and B, respectively (see above)) varies between 3.40 and 3.58 Å (for structures determined at resolutions between 1.40 Å and 1.80 Å, compared to a resolution of 1.75 Å for the structure of Rm3 presented here). With respect to other B3 enzymes, the main difference in the Rm3 active site is the positioning of the Wat2 water molecule (Figure 4b, c), which is notably closer to both Zn1 (distances 2.57 Å and 2.68 Å in Rm3 chains A and B, respectively) and Wat1 (2.33 Å and 1.96 Å) than is the case in e.g L1 (Wat2 – Zn1 and Wat2 – Wat1 distances 2.80 Å and 3.04 Å for pdb 1SML).

Implications of Rm3 Structure for Activity

Despite much effort, the precise mode of binding of β-lactams to the active site of B3 MBLs remains incompletely understood. In fact only one crystal structure has so far been determined for a B3 MBL complexed with antibiotic, that of L1 bound to the hydrolysis product of the oxacephem moxalactam (65); docking and quantum mechanics/molecular mechanics (QM/MM) approaches have been used to investigate interactions of AIM-1 with hydrolyzed cefoxitin (61). We therefore used superposition of the Rm3 and L1:moxalactam structures to consider possible

interactions of hydrolyzed moxalactam with Rm3 (Figure 6a, b) in an effort to investigate determinants of β-lactamase activity, and the basis for the high K_M values that are observed for β-lactam hydrolysis by Rm3.

Consistent with the ability of Rm3 to hydrolyze most classes of β-lactam, these comparisons imply that the enzyme can replicate many of the interactions with substrates made by L1 or AIM-1. In addition to interactions involving the two metal ions (Zn1 with the C7/C8 carbonyl/carboxylate of the β-lactam amide, and Zn2 with the C3/C4 carboxylate of the second ring), the Rm3 active site contains conserved residues at positions previously implicated in β-lactam binding. In particular, Ser221, a residue that is highly conserved in B3 MBLs, and Asn223 (Ser or Thr in most other B3 enzymes) are well positioned to contact the C3/C4 carboxylate of bound β-lactam. Notably, in the Rm3 crystal structure the anticipated positions adopted by the β-lactam carboxylate oxygen atoms are occupied by Wat2 and by a second water molecule (Wat3) positioned between the Ser221 and Asn223 side chains. As noted earlier, and as has been proposed for AIM-1 (61) and SMB-1 (57), the Gln157 side chain is positioned to contact the C7/C8 carboxylate generated by β-lactam hydrolysis. Furthermore, the conserved Trp41 side chain is able to make hydrophobic interactions with the β-lactam core. Rm3 is thus able to make productive interactions with the core components common across the different classes of β-lactam.

Given this apparent availability of productive modes of substrate binding, we then considered why Rm3 hydrolyzes β-lactams with relatively low efficiency. Inspection of molecular surfaces in the vicinity of the active site (Figure 6c, d) indicates that, compared to other B3 enzymes in which the active site sits in a relatively shallow groove, the Rm3 active site is positioned at the

bottom of a much deeper channel that runs across one side of the structure. Notably, the extended N-terminus forms one wall of this cleft in the region that would be expected to form the binding site for the C6/C7 (R1) substituent of β-lactams, either requiring substrates to adopt specific conformations on binding to avoid steric clashes, or necessitating significant conformational changes of the enzyme to render the active site more accessible to β-lactams, particularly those such as later generation cephalosporins (e.g. ceftazidime) with bulky C7 substituents. Interestingly, for the B3 MBL BJP-1, where in the unliganded enzyme the active site is occluded by the extended N-terminal α-helix, the crystal structure of a complex with a 4-nitrobenzenesulfonamide inhibitor showed that inhibitor binding involved displacement of this entire helix from its position in the native structure in order to make the active site accessible (53). We thus propose that the high K_M values for Rm3-catalyzed hydrolysis of β-lactams arise in large part from the steric constraints upon substrate binding that are imposed by the extended N-terminus. It is possible that the additional proline-rich N-terminal sequence, comprising a further 10 amino acids that could not be modeled in our final crystal structure, could impose further restrictions upon substrate binding.

Concluding Remarks

The increasing availability of sequence information from genomic and metagenomics projects has begun to establish the extent to which antibiotic resistance genes are distributed in the wider environment. It is now clear that MBLs, and the B3 subclass in particular, are frequently present on the chromosomes of environmental organisms that include, but are not limited to, opportunist human pathogens such as *S. maltophilia* or *E. meningosepticum*. Accumulating evidence shows

that the antibiotic era has been characterized by repeated instances of the mobilization of resistance determinants from environmental species, such as *Kluyvera* or *Shewanella* spp., into clinically significant pathogens, and their subsequent global dissemination on multiresistance plasmids. It is also becoming apparent that exposure to detergents and biocides, as well as antibiotics, may also be implicated in the mobilization of resistance genes, and co-selection of multiresistance elements. In this work we describe the properties of the product of a novel resistance gene, bla_{Rm3}, that was identified from an environment with high levels of biocide exposure.

bla_{Rm3} encodes a B3 MBL that is active against most β-lactam classes *in vitro* and is able to reduce the cephalosporin susceptibility of recombinant *E. coli*, thus replicating characteristics of enzymes of clinical importance. Sequence-based phylogeny indicates that Rm3 is representative of a distinct clade of B3 MBLs that differs from the L1 and FEZ-1/GOB groups (Figure 2). It is likely that, given their occurrence in environmental samples from sites that differ greatly in their geographical location and level of human impact, these enzymes have a wide distribution in the environment. With increasing use of broad-spectrum β-lactams, and the associated increase in selection pressure, there is thus considerable potential for future mobilization of MBLs of this type into the clinic. The structure of Rm3 demonstrates an overall resemblance to the mobilized AIM-1 and SMB-1 enzymes, and provides a basis both for the β-lactamase activity of Rm3 and the limited efficiency with which it hydrolyzes most substrates. However, the architecture of the active site that is created by the extended N-terminus distinguishes Rm3 from other B3 MBLs that have been studied so far, suggesting both that (as has been suggested for other B3 MBLs (50)) β-lactams may not necessarily be the natural substrates for these enzymes, and that there is

capacity for β-lactamase activity to be improved by mutation. Future experiments will investigate these possibilities.

Funding Information

R.S., J.S., J.B. and C.J.S. are supported by the U.K. Medical Research Council (U.K.-Canada Team Grant G1100135) and P.H. and J.S. by the National Institute of Allergy and Infectious Diseases of the U.S. National Institutes of Health under award number R01AI100560. LZ, WHG and EMHW were supported by NERC NE/E004482/1 and a European Regional Development Fund, grant no. 500020. The content is solely the responsibility of the authors and does not necessarily represent the official views of the National Institutes of Health.

Acknowledgements.

We thank Diamond Light Source for access to beamline I04 (proposal number MX313) that contributed to the results presented here.

References

1. **Fisher JF, Meroueh SO, Mobashery S.** 2005. Bacterial resistance to β-lactam antibiotics: compelling opportunism, compelling opportunity. *Chem Rev* **105:**395-424.
2. **Bush K.** 2013. Proliferation and significance of clinically relevant β-lactamases. Ann N Y Acad Sci **1277:**84-90.
3. **D'Andrea MM, Arena F, Pallecchi L, Rossolini GM.** 2013. CTX-M-type β-lactamases: a successful story of antibiotic resistance. Int J Med Microbiol **303:**305-317.
4. **Wellington EM, Boxall AB, Cross P, Feil EJ, Gaze WH, Hawkey PM, Johnson-Rollings AS, Jones DL, Lee NM, Otten W, Thomas CM, Williams AP.** 2013. The role of the natural environment in the emergence of antibiotic resistance in Gram-negative bacteria. Lancet Infect Dis **13:**155-165.
5. **Humeniuk C, Arlet G, Gautier V, Grimont P, Labia R, Philippon A.** 2002. β-lactamases of *Kluyvera ascorbata*, probable progenitors of some plasmid-encoded CTX-M types. Antimicrob Agents Chemother **46:**3045-3049.
6. **Poirel L, Kampfer P, Nordmann P.** 2002. Chromosome-encoded Ambler class A β-lactamase of *Kluyvera georgiana*, a probable progenitor of a subgroup of CTX-M extended-spectrum β-lactamases. Antimicrob Agents Chemother **46:**4038-4040.
7. **Sarria JC, Vidal AM, Kimbrough RC, 3rd.** 2001. Infections caused by *Kluyvera* species in humans. Clin Infect Dis **33:**E69-74.
8. **Ambler RP.** 1980. The structure of β-lactamases. Philos Trans R Soc Lond B Biol Sci **289:**321-331.
9. **Palzkill T.** 2013. Metallo-β-lactamase structure and function. Ann N Y Acad Sci **1277:**91-104.

10. **Crowder MW, Spencer J, Vila AJ.** 2006. Metallo-β-lactamases: novel weaponry for antibiotic resistance in bacteria. Acc Chem Res **39:**721-728.

11. **Drawz SM, Bonomo RA.** 2010. Three decades of β-lactamase inhibitors. Clin Microbiol Rev **23:**160-201.

12. **Dortet L, Poirel L, Nordmann P.** 2014. Worldwide dissemination of the NDM-type carbapenemases in Gram-negative bacteria. Biomed Res Int **2014:**249856.

13. **Papagiannitsis CC, Izdebski R, Baraniak A, Fiett J, Herda M, Hrabak J, Derde LP, Bonten MJ, Carmeli Y, Goossens H, Hryniewicz W, Brun-Buisson C, Gniadkowski M, Mosar Wp WP, groups WPs, Mosar Wp WP, groups WPs.** 2015. Survey of metallo-β-lactamase-producing Enterobacteriaceae colonizing patients in European ICUs and rehabilitation units, 2008-11. J Antimicrob Chemother **70:**1981-1988.

14. **Yong D, Toleman MA, Bell J, Ritchie B, Pratt R, Ryley H, Walsh TR.** 2012. Genetic and biochemical characterization of an acquired subgroup B3 metallo-β-lactamase gene, *bla*$_{AIM-1}$, and its unique genetic context in *Pseudomonas aeruginosa* from Australia. Antimicrob Agents Chemother **56:**6154-6159.

15. **Wachino J, Yoshida H, Yamane K, Suzuki S, Matsui M, Yamagishi T, Tsutsui A, Konda T, Shibayama K, Arakawa Y.** 2011. SMB-1, a novel subclass B3 metallo-β-lactamase, associated with ISCR1 and a class 1 integron, from a carbapenem-resistant *Serratia marcescens* clinical isolate. Antimicrob Agents Chemother **55:**5143-5149.

16. **Bicknell R, Emanuel EL, Gagnon J, Waley SG.** 1985. The production and molecular properties of the zinc β-lactamase of *Pseudomonas maltophilia* IID 1275. Biochem J **229:**791-797.

528 17. **Bellais S, Aubert D, Naas T, Nordmann P.** 2000. Molecular and biochemical
529 heterogeneity of class B carbapenem-hydrolyzing β-lactamases in *Chryseobacterium*
530 *meningosepticum*. Antimicrob Agents Chemother **44:**1878-1886.
531 18. **Bebrone C.** 2007. Metallo-β-lactamases (classification, activity, genetic organization,
532 structure, zinc coordination) and their superfamily. Biochem Pharmacol **74:**1686-1701.
533 19. **Gaze WH, Krone SM, Larsson DG, Li XZ, Robinson JA, Simonet P, Smalla K,**
534 **Timinouni M, Topp E, Wellington EM, Wright GD, Zhu YG.** 2013. Influence of
535 humans on evolution and mobilization of environmental antibiotic resistome. Emerg
536 Infect Dis **19**.
537 20. **Allen HK, Moe LA, Rodbumrer J, Gaarder A, Handelsman J.** 2009. Functional
538 metagenomics reveals diverse β-lactamases in a remote Alaskan soil. ISME J **3:**243-251.
539 21. **Amos GC, Zhang L, Hawkey PM, Gaze WH, Wellington EM.** 2014. Functional
540 metagenomic analysis reveals rivers are a reservoir for diverse antibiotic resistance genes.
541 Vet Microbiol **171:**441-447.
542 22. **Torres-Cortes G, Millan V, Ramirez-Saad HC, Nisa-Martinez R, Toro N, Martinez-**
543 **Abarca F.** 2011. Characterization of novel antibiotic resistance genes identified by
544 functional metagenomics on soil samples. Environ Microbiol **13:**1101-1114.
545 23. **Shoemaker WR, Muscarella ME, Lennon JT.** 2015. Genome Sequence of the Soil
546 Bacterium *Janthinobacterium* sp. KBS0711. Genome Announc **3**.
547 24. **Forsberg KJ, Patel S, Gibson MK, Lauber CL, Knight R, Fierer N, Dantas G.** 2014.
548 Bacterial phylogeny structures soil resistomes across habitats. Nature **509:**612-616.

Antimicrobial Agents and Chemotherapy

549 25. **Docquier JD, Lopizzo T, Liberatori S, Prenna M, Thaller MC, Frere JM, Rossolini**
550 **GM.** 2004. Biochemical characterization of the THIN-B metallo-β-lactamase of
551 *Janthinobacterium lividum*. Antimicrob Agents Chemother **48:**4778-4783.
552 26. **Stoczko M, Frere JM, Rossolini GM, Docquier JD.** 2006. Postgenomic scan of
553 metallo-β-lactamase homologues in rhizobacteria: identification and characterization of
554 BJP-1, a subclass B3 ortholog from *Bradyrhizobium japonicum*. Antimicrob Agents
555 Chemother **50:**1973-1981.
556 27. **Gaze WH, Abdouslam N, Hawkey PM, Wellington EM.** 2005. Incidence of class 1
557 integrons in a quaternary ammonium compound-polluted environment. Antimicrob
558 Agents Chemother **49:**1802-1807.
559 28. **Newman JR, Fuqua C.** 1999. Broad-host-range expression vectors that carry the L-
560 arabinose-inducible *Escherichia coli* araBAD promoter and the araC regulator. Gene
561 **227:**197-203.
562 29. **Andrews JM.** 2001. Determination of minimum inhibitory concentrations. J Antimicrob
563 Chemother **48, Supplement 1:**5-16.
564 30. **Studier FW, Rosenberg AH, Dunn JJ, Dubendorff JW.** 1990. Use of T7 RNA
565 polymerase to direct expression of cloned genes. Methods Enzymol **185:**60-89.
566 31. **Laemmli UK.** 1970. Cleavage of structural proteins during the assembly of the head of
567 bacteriophage T4. Nature **227:**680-685.
568 32. **Brem J, Struwe WB, Rydzik AM, Tarhonskaya H, Pfeffer I, Flashman E, van**
569 **Berkel SS, Spencer J, Claridge TD, McDonough MA, Benesch JL, Schofield CJ.**
570 2015. Studying the active-site loop movement of the Sao Paolo metallo-β-lactamase-1.
571 Chem Sci **6:**956-963.

572 33. **Wilkins MR, Gasteiger E, Bairoch A, Sanchez JC, Williams KL, Appel RD,**
573 **Hochstrasser DF.** 1999. Protein identification and analysis tools in the ExPASy server.
574 Methods Mol Biol **112:**531-552.
575 34. **Laraki N, Franceschini N, Rossolini GM, Santucci P, Meunier C, de Pauw E,**
576 **Amicosante G, Frere JM, Galleni M.** 1999. Biochemical characterization of the
577 *Pseudomonas aeruginosa* 101/1477 metallo-β-lactamase IMP-1 produced by *Escherichia*
578 *coli*. Antimicrob Agents Chemother **43:**902-906.
579 35. **Toth M, Vakulenko V, Antunes NT, Frase H, Vakulenko SB.** 2012. Class A
580 carbapenemase FPH-1 from *Francisella philomiragia*. Antimicrob Agents Chemother
581 **56:**2852-2857.
582 36. **Radaev S, Li S, Sun PD.** 2006. A survey of protein-protein complex crystallizations.
583 Acta Crystallogr D Biol Crystallogr **62:**605-612.
584 37. **Kabsch W.** 2010. XDS. Acta Crystallogr D Biol Crystallogr **66:**125-132.
585 38. **Evans PR.** 2011. An introduction to data reduction: space-group determination, scaling
586 and intensity statistics. Acta Crystallogr D Biol Crystallogr **67:**282-292.
587 39. **Winter G.** 2010. xia2: an expert system for macromolecular crystallography data
588 reduction. Journal of Applied Crystallography **43:**186-190.
589 40. **McCoy AJ, Grosse-Kunstleve RW, Adams PD, Winn MD, Storoni LC, Read RJ.**
590 2007. Phaser crystallographic software. J Appl Cryst **40:**658-674.
591 41. **Stein N.** 2008. CHAINSAW: a program for mutating pdb files used as templates in
592 molecular replacement. Journal of Applied Crystallography **41:**641-643.
593 42. **Lienard BM, Garau G, Horsfall L, Karsisiotis AI, Damblon C, Lassaux P,**
594 **Papamicael C, Roberts GC, Galleni M, Dideberg O, Frere JM, Schofield CJ.** 2008.

595 Structural basis for the broad-spectrum inhibition of metallo-β-lactamases by thiols. Org
596 Biomol Chem **6:**2282-2294.
597 43. **Emsley P, Lohkamp B, Scott WG, Cowtan K.** 2010. Features and development of
598 Coot. Acta Crystallogr D Biol Crystallogr **66:**486-501.
599 44. **Murshudov GN, Vagin AA, Dodson EJ.** 1997. Refinement of Macromolecular
600 Structures by the Maximum-Likelihood Method. Acta Crystallogr D Biol Crystallogr
601 **53:**240-255.
602 45. **Chen VB, Arendall WB, 3rd, Headd JJ, Keedy DA, Immormino RM, Kapral GJ,**
603 **Murray LW, Richardson JS, Richardson DC.** 2010. MolProbity: all-atom structure
604 validation for macromolecular crystallography. Acta Crystallogr D Biol Crystallogr
605 **66:**12-21.
606 46. **Adams PD, Afonine PV, Bunkoczi G, Chen VB, Davis IW, Echols N, Headd JJ,**
607 **Hung LW, Kapral GJ, Grosse-Kunstleve RW, McCoy AJ, Moriarty NW, Oeffner R,**
608 **Read RJ, Richardson DC, Richardson JS, Terwilliger TC, Zwart PH.** 2010.
609 PHENIX: a comprehensive Python-based system for macromolecular structure solution.
610 Acta Crystallogr D Biol Crystallogr **66:**213-221.
611 47. **Pal C, Bengtsson-Palme J, Kristiansson E, Larsson DG.** 2015. Co-occurrence of
612 resistance genes to antibiotics, biocides and metals reveals novel insights into their co-
613 selection potential. BMC Genomics **16:**964.
614 48. **Buffet-Bataillon S, Tattevin P, Bonnaure-Mallet M, Jolivet-Gougeon A.** 2012.
615 Emergence of resistance to antibacterial agents: the role of quaternary ammonium
616 compounds--a critical review. Int J Antimicrob Agents **39:**381-389.

617 49. **Petersen TN, Brunak S, von Heijne G, Nielsen H.** 2011. SignalP 4.0: discriminating
618 signal peptides from transmembrane regions. Nat Methods **8:**785-786.

619 50. **Stoczko M, Frere JM, Rossolini GM, Docquier JD.** 2008. Functional diversity among
620 metallo-β-lactamases: characterization of the CAR-1 enzyme of *Erwinia carotovora*.
621 Antimicrob Agents Chemother **52:**2473-2479.

622 51. **Docquier JD, Pantanella F, Giuliani F, Thaller MC, Amicosante G, Galleni M, Frere**
623 **JM, Bush K, Rossolini GM.** 2002. CAU-1, a subclass B3 metallo-β-lactamase of low
624 substrate affinity encoded by an ortholog present in the *Caulobacter crescentus*
625 chromosome. Antimicrob Agents Chemother **46:**1823-1830.

626 52. **Galleni M, Lamotte-Brasseur J, Rossolini GM, Spencer J, Dideberg O, Frere JM.**
627 2001. Standard numbering scheme for class B β-lactamases. Antimicrob Agents
628 Chemother **45:**660-663.

629 53. **Docquier J-D, Benvenuti M, Calderone V, Stoczko M, Menciassi N, Rossolini GM,**
630 **Mangani S.** 2010. High-resolution crystal structure of the subclass B3 metallo-β-
631 lactamase BJP-1: rational basis for substrate specificity and interaction with
632 sulfonamides. Antimicrob Agents Chemother **54:**4343-4351.

633 54. **Page MI, Badarau A.** 2008. The mechanisms of catalysis by metallo β-lactamases.
634 Bioinorg Chem Appl doi:10.1155/2008/576297**:**576297.

635 55. **Addison AW, Rao TN, Reedijk J, Vanrijn J, Verschoor GC.** 1984. Synthesis,
636 Structure, and Spectroscopic Properties of Copper(Ii) Compounds Containing Nitrogen
637 Sulfur Donor Ligands - the Crystal and Molecular-Structure of Aqua[1,7-Bis(N-
638 Methylbenzimidazol-2'-Yl)-2,6-Dithiaheptane]Copper(Ii) Perchlorate. Journal of the
639 Chemical Society-Dalton Transactions doi:Doi 10.1039/Dt9840001349**:**1349-1356.

Antimicrobial Agents and Chemotherapy

56. **Yamaguchi Y, Takashio N, Wachino J, Yamagata Y, Arakawa Y, Matsuda K, Kurosaki H.** 2010. Structure of metallo-β-lactamase IND-7 from a *Chryseobacterium indologenes* clinical isolate at 1.65-Å resolution. J Biochem **147:**905-915.

57. **Wachino J, Yamaguchi Y, Mori S, Kurosaki H, Arakawa Y, Shibayama K.** 2013. Structural insights into the subclass B3 metallo-β-lactamase SMB-1 and the mode of inhibition by the common metallo-β-lactamase inhibitor mercaptoacetate. Antimicrob Agents Chemother **57:**101-109.

58. **Krissinel E, Henrick K.** 2004. Secondary-structure matching (SSM), a new tool for fast protein structure alignment in three dimensions. Acta Crystallogr D Biol Crystallogr **60:**2256-2268.

59. **Ullah JH, Walsh TR, Taylor IA, Emery DC, Verma CS, Gamblin SJ, Spencer J.** 1998. The crystal structure of the L1 metallo-β-lactamase from *Stenotrophomonas maltophilia* at 1.7 Å resolution. J Mol Biol **284:**125-136.

60. **Garcia-Saez I, Mercuri PS, Papamicael C, Kahn R, Frere JM, Galleni M, Rossolini GM, Dideberg O.** 2003. Three-dimensional structure of FEZ-1, a monomeric subclass B3 metallo-β-lactamase from *Fluoribacter gormanii*, in native form and in complex with D-captopril. J Mol Biol **325:**651-660.

61. **Leiros HK, Borra PS, Brandsdal BO, Edvardsen KS, Spencer J, Walsh TR, Samuelsen O.** 2012. Crystal structure of the mobile metallo-β-lactamase AIM-1 from *Pseudomonas aeruginosa*: insights into antibiotic binding and the role of Gln157. Antimicrob Agents Chemother **56:**4341-4353.

661 62. **Carenbauer AL, Garrity JD, Periyannan G, Yates RB, Crowder MW.** 2002. Probing
662 substrate binding to Metallo-β-Lactamase L1 from *Stenotrophomonas maltophilia* by
663 using site-directed mutagenesis. BMC Biochem **3:**4.

664 63. **Mercuri PS, Garcia-Saez I, De Vriendt K, Thamm I, Devreese B, Van Beeumen J,**
665 **Dideberg O, Rossolini GM, Frere JM, Galleni M.** 2004. Probing the specificity of the
666 subclass B3 FEZ-1 metallo-β-lactamase by site-directed mutagenesis. J Biol Chem
667 **279:**33630-33638.

668 64. **Garrity JD, Carenbauer AL, Herron LR, Crowder MW.** 2004. Metal binding Asp-
669 120 in metallo-β-lactamase L1 from *Stenotrophomonas maltophilia* plays a crucial role in
670 catalysis. J Biol Chem **279:**920-927.

671 65. **Spencer J, Read J, Sessions RB, Howell S, Blackburn GM, Gamblin SJ.** 2005.
672 Antibiotic recognition by binuclear metallo-β-lactamases revealed by X-ray
673 crystallography. J Am Chem Soc **127:**14439-14444.

674 66. **Crowder MW, Walsh TR, Banovic L, Pettit M, Spencer J.** 1998. Overexpression,
675 purification, and characterization of the cloned metallo-β-lactamase L1 from
676 *Stenotrophomonas maltophilia*. Antimicrob Agents Chemother **42:**921-926.

677 67. **Simm AM, Higgins CS, Carenbauer AL, Crowder MW, Bateson JH, Bennett PM,**
678 **Clarke AR, Halford SE, Walsh TR.** 2002. Characterization of monomeric L1 metallo-β
679 -lactamase and the role of the N-terminal extension in negative cooperativity and
680 antibiotic hydrolysis. J Biol Chem **277:**24744-24752.

681 68. **Spencer J, Clarke AR, Walsh TR.** 2001. Novel mechanism of hydrolysis of therapeutic
682 beta-lactams by *Stenotrophomonas maltophilia* L1 metallo-β-lactamase. J Biol Chem
683 **276:**33638-33644.

69. **Mercuri PS, Bouillenne F, Boschi L, Lamotte-Brasseur J, Amicosante G, Devreese B, van Beeumen J, Frere JM, Rossolini GM, Galleni M.** 2001. Biochemical characterization of the FEZ-1 metallo-β-lactamase of *Legionella gormanii* ATCC 33297T produced in *Escherichia coli*. Antimicrob Agents Chemother **45:**1254-1262.

70. **Sievers F, Wilm A, Dineen D, Gibson TJ, Karplus K, Li W, Lopez R, McWilliam H, Remmert M, Soding J, Thompson JD, Higgins DG.** 2011. Fast, scalable generation of high-quality protein multiple sequence alignments using Clustal Omega. Mol Syst Biol **7:**539.

71. **Kabsch W, Sander C.** 1983. Dictionary of protein secondary structure: pattern recognition of hydrogen-bonded and geometrical features. Biopolymers **22:**2577-2637.

72. **Robert X, Gouet P.** 2014. Deciphering key features in protein structures with the new ENDscript server. Nucleic Acids Res **42:**W320-324.

73. **Felsenstein J.** 1989. PHYLIP - Phylogeny Inference Package (Version 3.2). Cladistics **5:**164 - 166.

Table 1. Effect of RM3 Expression on β-lactam MICs (μg / ml) for Recombinant *Escherichia coli* EC100.

	AMP	AMX	CAR	TMC	ATM	CTX	CAZ	IPM
pCF430[a]	8	8	32	16	0.25	0.25	0.5	0.5
pCF430:RM3[b]	16	8	32	32	0.5	0.25	8	1

[a] MIC values of empty pCF430 in *Escherichia coli* EC100.

[b] MIC values for pCF430 carrying 8 kb RM3 metagenomic fragment

AMP = ampicillin, AMX = amoxicillin, CAR = carbenicillin, TMC = temocillin, ATM = aztreonam, CTX = Cefotaxime, CAZ = Ceftazidime, IPM = imipenem.

708 **Table 2. Kinetic parameters for Hydrolysis of Selected β-Lactams by Rm3 and Selected B3 MBLs.**

	Rm3			L1			FEZ-1 [d]			BJP-1 [e]			AIM-1 [f]			SMB-1 [g]		
β-lactam	K_M [a]	k_{cat} [b]	k_{cat}/K_M [c]	K_M [a]	k_{cat} [b]	k_{cat}/K_M [c]	K_M [a]	k_{cat} [b]	k_{cat}/K_M [c]	K_M [a]	k_{cat} [b]	k_{cat}/K_M [c]	K_M [a]	k_{cat} [b]	k_{cat}/K_M [c]	K_M [a]	k_{cat} [b]	k_{cat}/K_M [c]
Penicillin G	ND	ND	4.1 x 10^4	75 ±10*	410 ±20	5.5 x 10^6	590 ±70	70 ±5	1.1 x 10^5	130	18	1.3 x 10^5	31	778	2.6 x 10^7	ND	ND	ND
Ampicillin	1600 ±260	33.6 ±3	2.1 x 10^4	300 ±15	580 ±20	1.9 x 10^6	>5000	>5.5	1.1 x 10^4	670	13	1.9 x 10^4	41	594	1.4 x 10^6	102	247	2.4 x 10^6
Cefoxitin	ND	ND	1.5 x 10^4	3.3 ±0.4*	2.2 ±0.1	6.7 x 10^5	11 ±1	3 ±0.5	2.7 x 10^5	140	10	7.1 x 10^4	26	145	5.7 x 10^6	26	39	1.5 x 10^6
Ceftazidime	ND	ND	2.1 x 10^4	145 ±13**	27 ±3	2.0 x 10^5	>1000	>4	4.0 x 10^3	>700	>3	4.3 x 10^3	148	7	4.9 x 10^4	57	4.4	7.7 x 10^4
Cefotaxime	ND	ND	7.1 x 10^4	160 ±20*	140 ±9	8.8 x 10^5	70 ±8	165 ±15	2.4 x 10^6	300	41	1.4 x 10^5	49	609	1.2 x 10^7	35	31	8.9 x 10^5
Meropenem	232 ± 9	8.9 ±0.2	3.8 x 10^4	13 ***	77	5.9 x 10^6	85 ±3	45 ±2	5.0 x 10^5	190	156	8.3 x 10^5	163	1000	6.8 x 10^6	144	604	4.2 x 10^6
Imipenem	ND	ND	1.0 x 10^4	48 ±8**	384 ±6	8 x 10^6	>1000	>200	2.0 x 10^5	260	15	6.0 x 10^4	97	1700	1.7 x 10^7	133	518	3.9 x 10^6
Aztreonam	NH	ND	ND	ND	ND	ND	>1000	$<10^{-2}$	<10	NH	ND	ND	NH	ND	ND	NH	ND	ND

709 [a] μM [b] s^{-1} [c] M^{-1} s^{-1}

710 Kinetic data for L1 are from (66)*, (67)**, (68)***.

711 Kinetic data for other enzymes are from FEZ-1 (69), BJP-1 (26), AIM-1 (14) and SMB-1 (15).

712

713

714 **Table 3. Crystallographic Data Collection and Refinement Statistics**

Data Collection	
Beamline	DLS (I04)
Wavelength (Å)	0.9795
Space Group	$P2_1$
Cell Dimensions	
a, *b*, *c* (Å)	45.88, 74.45, 77.46
α, β, γ	90, 99.48, 90
Molecules/asymmetric unit	2
Resolution (Å)	53.32 - 1.75 (1.78 – 1.75)[a]
No. of unique reflections	50630 (2761)[a]
Redundancy	2.4 (2.3)[a]
R_{merge}	0.055 (0.363)[a]
CC1/2	0.997 (0.821)[a]
I/σ	9.1 (2.1)[a]
Completeness (%)	97.6 (97.2)[a]
Refinement	
Resolution (Å)	53.32 - 1.75 (1.78 – 1.75)[a]
No. of reflections	50593 (2780)[a]
R_{work}/R_{free}[b]	20.28 / 22.94 (31.15 / 32.18)[a]
No. Protein atoms	2022[c] / 2029[d]
No. Zinc ions	7
No. Water molecules	302
B factors (protein)	25.58[c] / 26.65[d]
B-factor (zinc)	19.38
B-factor (water)	29.25
Bond length rmsd (Å)	0.007
Bond angle rmsd (°)	1.09

715 [a]Highest resolution shell statistics are shown in parentheses.

716 [b]R_{free} was calculated with 5% of reflections omitted from refinement

717 [c]chain A

718 [d]chain B

Antimicrobial Agents and Chemotherapy

Figure 1: Sequence Alignment of SubClass B3 Metallo-β-Lactamases. Alignment of selected subclass B3 MBLs. Sequences were aligned using ClustalOmega (70) invariant residues are highlighted with a red background, conservative substitutions are in red text. Residue numbering is according to the BBL standard numbering scheme (52); discontinuities (e.g. between residues 5- 70 , 80 – 90 and 150 – 170) are due to omission from the Figure of other MBL subclasses. Secondary structure assignments (DSSP; (71)) are from Rm3 structure (this work). Zinc binding residues are indicated by red triangles. Cysteine pairs 208 and 213, and 256 and 290 are labeled 1 and 2, respectively. Positions of key Rm3 residues and of Rm3 loops 1 and 2 are labeled below the alignment. This Figure was prepared using EsPript (72).

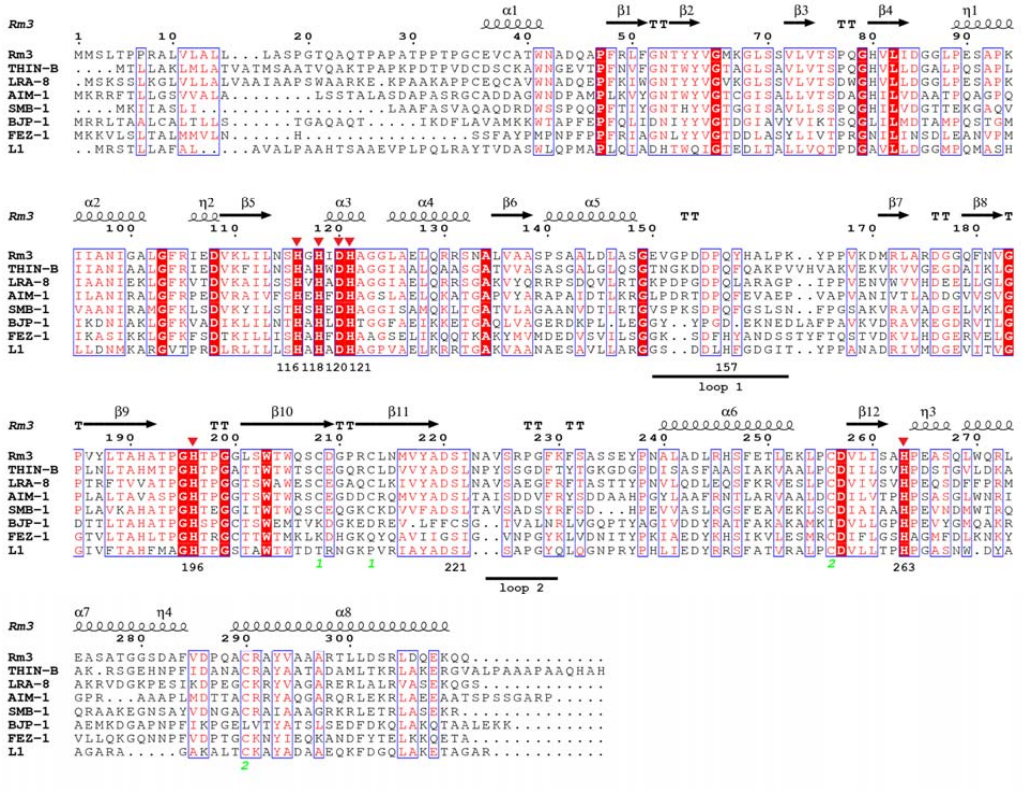

731 **Figure 2: Phylogenetic Tree of Selected Subclass B3 Metallo-β-Lactamases.** Sequences were
732 aligned using ClustalOmega (70) and the phylogenetic tree was visualized using the Drawgram
733 3.67 component of the PHYLIP package (73).

734

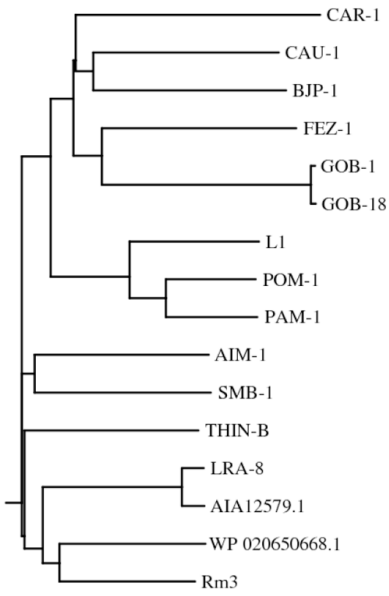

735

736

Figure 3: Overall Structure of Rm3. Stereo view of Rm3, with protein backbone color-ramped from blue (N-) to red (C-terminus). Active site residues and disulfide bonds are rendered as sticks (carbon atoms in green, other atom colors as standard). Zinc ions (gray) and water molecules (red) are shown as spheres. This Figure was generated using Pymol (www.pymol.org).

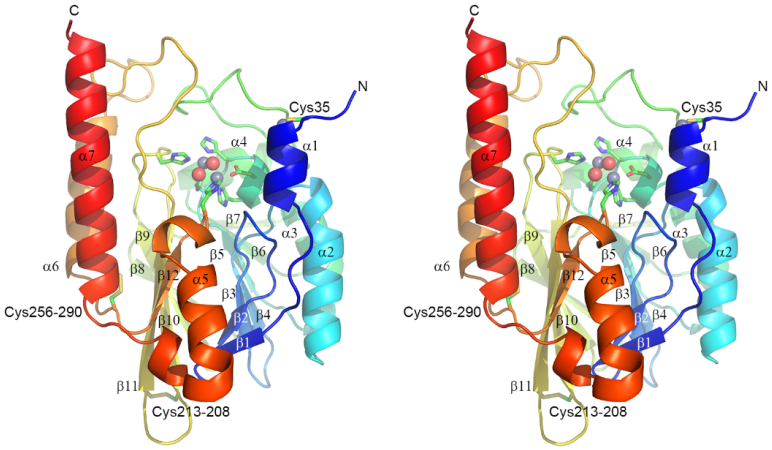

744 **Figure 4: Rm3 Active Site.** A. Stereoview; carbon atoms are colored green, zinc ions gray,
745 water molecules red, other colors as standard. Electron density map is 2|Fo| - |Fc|.ϕ_{calc}, contoured
746 at 1.5 σ. B. Active site of Rm3 showing position of Wat2 relative to Zn1 (distance in black) and
747 Wat1 (distance in white). C. Active site of L1 (pdb 1SML, (59)) showing position of Wat2
748 relative to Zn1 and Wat1. This Figure was generated using Pymol.

749

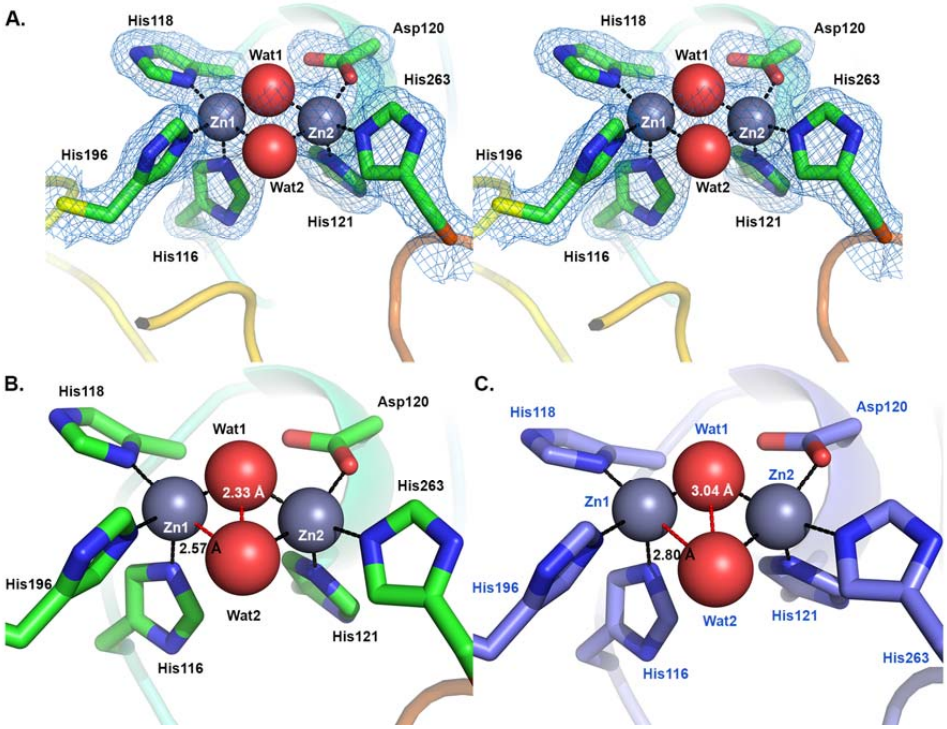

750

751

752 **Figure 5. Comparison of Rm3 with Other B3 MBLs**. Superposition of Rm3 structure upon
753 those of other B3 MBLs. A. Overall fold of Rm3 (chain A; color-ramped from N- (blue) to C-
754 (red) terminus. B. SMB-1 (pdb 3VPE (57)). C. L1 (pdb 1SML (59)). D. BJP-1 (pdb 3LVZ (53)).
755 Residues discussed in the text are rendered as sticks. This Figure was generated using Pymol.

756

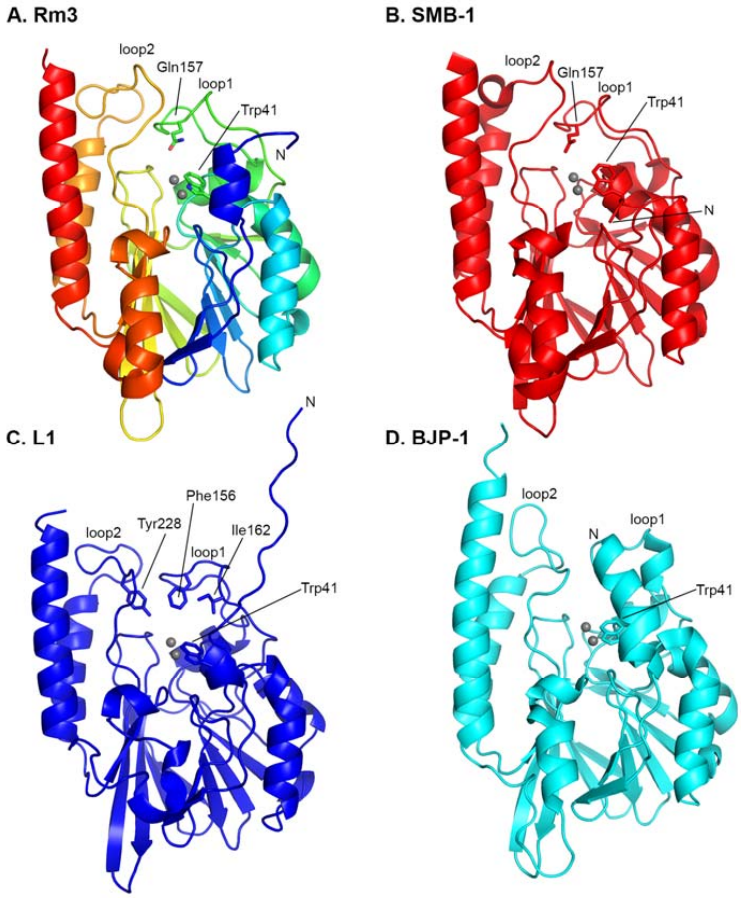

757

758

Antimicrobial Agents and Chemotherapy

759 **Figure 6: Proposed Interactions of Rm3 with Substrates**. A. Crystal structure of L1 bound to
760 hydrolyzed moxalactam (pdb 2AIO; (65)). B. Superposition of hydrolyzed moxalactam from pdb
761 2AI0 on structure of Rm3 (this work). Note that superposition places the moxalactam C4
762 carboxylate over Wat2 and Wat3, N5 and the C4 carboxylate in proximity to Zn2 and the C8
763 carboxylate close to Zn1. C. and D. space-filling representations of the L1 complex (pdb 2AIO)
764 and Rm3 structure (this work) with bound moxalactam superposed in stick form. The extended
765 N-terminus of Rm3 (residues 32 - 43) is highlighted in pale green. This Figure was generated
766 using Pymol.

767

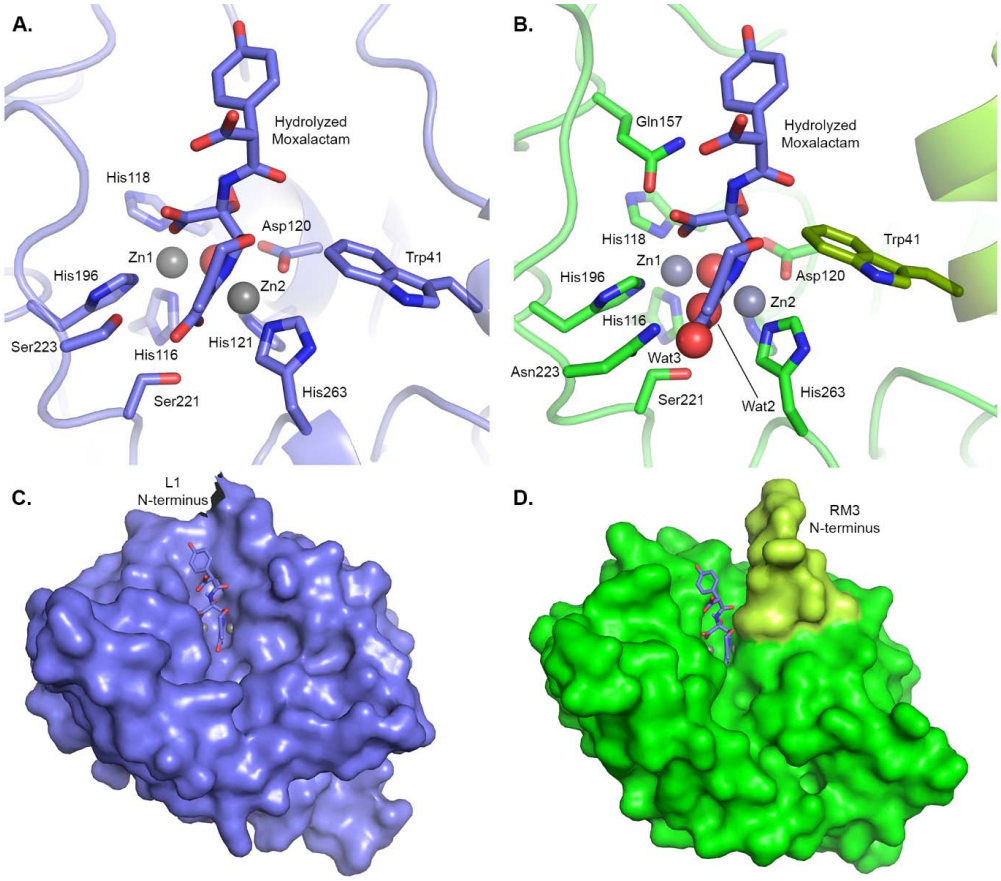

768

769

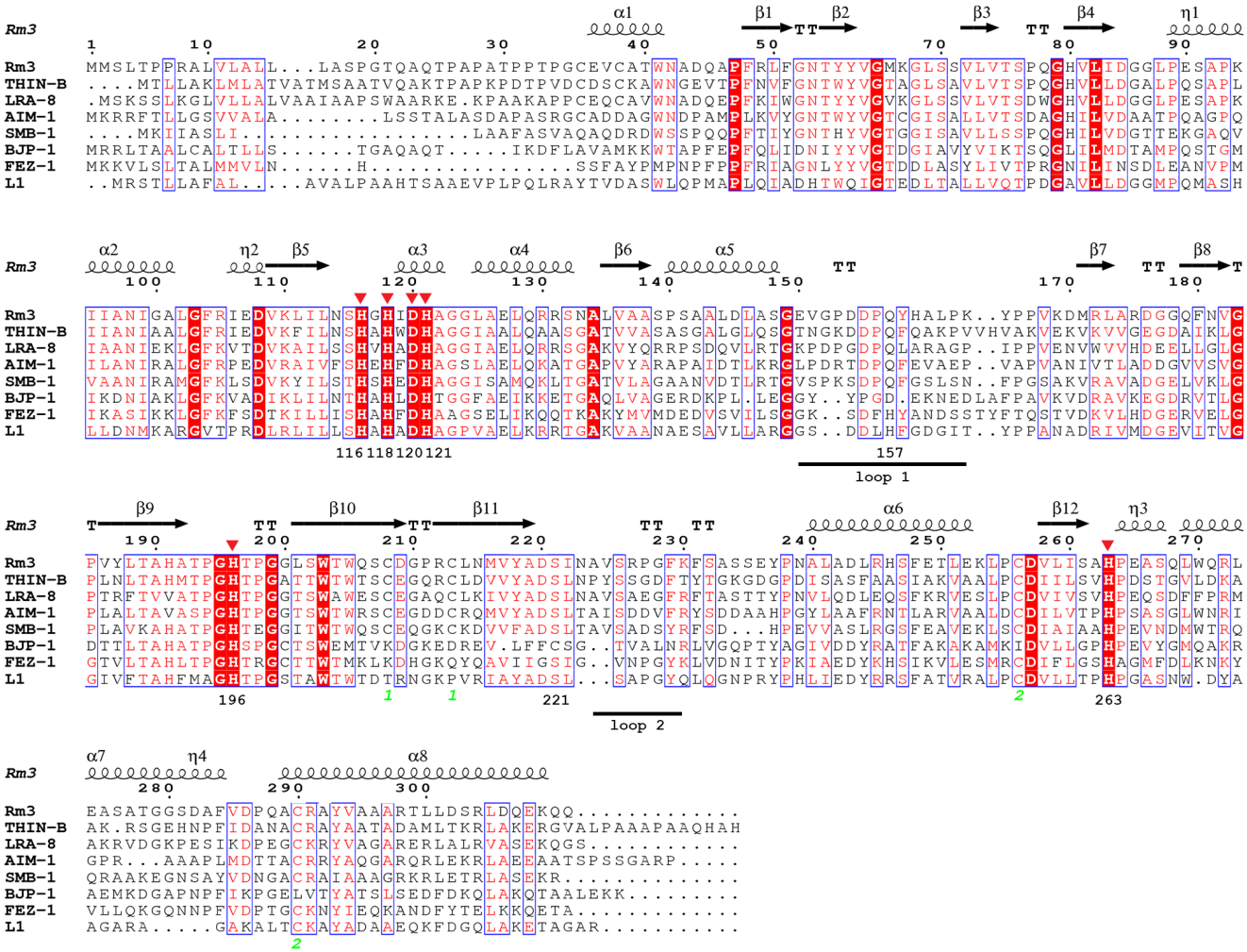

Antimicrobial Agents and Chemotherapy